NJC

Accepted Manuscript

This is an *Accepted Manuscript*, which has been through the Royal Society of Chemistry peer review process and has been accepted for publication.

Accepted Manuscripts are published online shortly after acceptance, before technical editing, formatting and proof reading. Using this free service, authors can make their results available to the community, in citable form, before we publish the edited article. We will replace this *Accepted Manuscript* with the edited and formatted *Advance Article* as soon as it is available.

You can find more information about *Accepted Manuscripts* in the Information for Authors.

Please note that technical editing may introduce minor changes to the text and/or graphics, which may alter content. The journal's standard Terms & Conditions and the Ethical guidelines still apply. In no event shall the Royal Society of Chemistry be held responsible for any errors or omissions in this *Accepted Manuscript* or any consequences arising from the use of any information it contains.

ROYAL SOCIETY OF CHEMISTRY

www.rsc.org/njc

From Ni-based nanoprecursors to NiO nanostructures: Morphology-controlled synthesis and structure-dependent electrochemical behavior

Gang Cheng [a], Yinan Yan [b], and Rong Chen [a]**

[a] School of Chemistry and Environmental Engineering, Wuhan Institute of Technology, Xiongchu Avenue, Wuhan, 430073, P. R. China.

[b] National Engineering Research Center for Nanotechnology, Shanghai, 200241, P. R. China.

* Corresponding author: gchenglab@163.com; rchenhku@hotmail.com

Abstract

A phase transformation and morphology tailoring of NiO nanostructures have been successfully achieved from Ni-based precursors ($Ni(SO_4)_{0.3}(OH)_{1.4}$ and $Ni(HCO_3)_2$) synthesized by a facile urea-controlled hydrothermal route. The as-synthesized NiO nanomaterials were characterized by X-ray diffraction (XRD), X-ray photoelectron spectroscopy (XPS), field emission scanning electron microscopy (FESEM), transmission electron microscopy (TEM), and nitrogen adsorption analyses. The electrochemical performance of the as-prepared NiO nanostructures was evaluated by CV and galvanostatic charge–discharge tests. NiO nanoparticles with larger surface areas exhibited higher electrochemical performance than nanobelts and nanospheres when used as the supercapacitor electrodes. The discharge capacity of NiO nanoparticles can retain 609.5 F g^{-1} after 500 cycles at a charging/discharging current density of 5 A g^{-1}.

1. Introduction

Supercapacitors have attracted considerable attention in the past decade as they have the potential to satisfy the demand of high power density in many advanced technologies.[1, 2] Nickel oxide (NiO) is regard as one of promising supercapacitor materials because of its excellent electrochemical properties and potential application in electrodes.[3-7] In particular, engineering NiO materials at the nanoscale offers unique properties resulting in high performance electrodes in energy storage devices. Consequently, considerable efforts have been made in recent years to fulfill the future requirements of electrochemical energy storage using NiO-based nanomaterials. At the same time, study on the intrinsic relationship between structure/size and property has engendered an urgent need for adjustable synthetic strategies,[8, 9] where the particle size and morphology of NiO nanomaterials can be precisely controlled with designed functionalities.

Being one of the most commonly used methods, thermal decomposition of $Ni(OH)_2$ intermediate has been widely employed to synthesize NiO nanostructures.[10, 11] Such as Cui et al. fabricated lotus-root-like NiO nanosheets and flower-like NiO microspheres through a calcination treatment of $Ni(OH)_2$ nanosheets and microspheres precursors, respectively.[12] However, such a synthetic technique for preparing nanostructured NiO materials, especially achieving control of morphology and structure, still remains a challenge because the morphology of the as-synthesized $Ni(OH)_2$ is mainly in the form of two dimensional and three dimensional nanostructures, including nanosheets,[5] nanoflakes,[13] and hierarchical nanostructures.[14] Although much attention has been paid on structures control of $Ni(OH)_2$ nanomaterials using ionic liquids, surfactants, templates,[15-18] most of the methods suffered

from drawbacks such as complicated shape-control processes because of involving of other additives. On the other hand, substantial efforts have been made toward the development of choosing a new suitable Ni-based nanoprecursor with a proper transformation process to selectively prepare NiO with special shapes and structures.[19-21] However, there are few publications relevant to tunable fabrication of NiO nanostructures and investigation on the effect of structure/morphology on the electrochemical performance.

Herein, we have successfully synthesized Ni-based nanostructures precursors including $Ni(SO_4)_{0.3}(OH)_{1.4}$ and $Ni(HCO_3)_2$ by a facile urea-controlled hydrothermal approach. At the same time, we have achieved a phase transformation and morphology tailoring of NiO nanomaterials from the as-synthesized Ni-based precursors. In addition, the electrochemical performances of the as-prepared NiO nanostructures with different morphologies were also evaluated.

2. Experimental section

All of the reagents were of analytical grade and were used without further purification. De-ionized water was used for all experiments.

The $Ni(SO_4)_{0.3}(OH)_{1.4}$ and $Ni(HCO_3)_2$ nanostructures precursors was synthesized by a facile urea-controlled hydrothermal method. In a typical synthesis, 2 mmol of $NiSO_4{\cdot}(NH_4)_2SO_4{\cdot}6H_2O$ and a proper amount of urea was added to 30 mL of deionized water, and then sonicated until a transparent solution was formed. After that, the homogeneous solution was transferred into a 50 mL Teflon-lined autoclave and maintained the temperature at 180°C for 18 h. After cooling down to room temperature, the products were collected and washed with de-ionized water and ethanol several times by centrifugation. The final product was dried for 12 h at 80°C. The mole ratios of $NiSO_4{\cdot}(NH_4)_2SO_4{\cdot}6H_2O$ with respect to the urea were 1:1, 1:6, and 1:15, which are referred as P1, P2, and P3, respectively.

NiO nanomaterials with different morphologies were prepared by calcining of $Ni(SO_4)_{0.3}(OH)_{1.4}$ and $Ni(HCO_3)_2$ nanostructures precursors at 450°C for 2 h in air at a ramping rate of 4 °C min^{-1}.

The as-synthesized Ni-based nanostructures were characterized by powder X-ray diffraction (XRD), scanning electron microscopy (SEM), and transmission electron microscopy (TEM). XRD was performed using a D8 Advance (Bruker, Germany) at room temperature in specular reflection mode with Cu/Kα radiation at a scanning rate of 0.03° s^{-1} in the 2θ range from 20° to 90°. SEM images were taken on a field-emission electron

microscope S4800 operating at an acceleration voltage of 5 kV. TEM images were recorded on a JEOL 2010 electron microscope at an accelerating voltage of 200 kV. The Brunauer–Emmett–Teller (BET) specific surface areas of the powders were determined by nitrogen adsorption in a Micromeritics ASAP 2020 nitrogen adsorption apparatus (USA).

Electrochemical performance was recorded by computer-controlled CH660D electrochemical work station (CHI instruments Inc., USA) equipped with two compartments and three electrode cells. Platinum gauze was used as current collector for the work electrode, and platinum foil and saturated calomel electrode was used as the auxiliary electrode and reference electrode, respectively. For preparing the working electrode, the electro-active material (NiO, 85 wt %), acetylene black (10 wt %), and poly(tetrafluoroethylene) (5 wt %) was firstly mixed together, then a few drops of ethanol were added to form homogeneous slurry and finally the slurry was pressed and pasted on the platinum gauze with mass of 5 mg. All electrochemical measurements were carried out in a 6M KOH solution as the electrolyte.

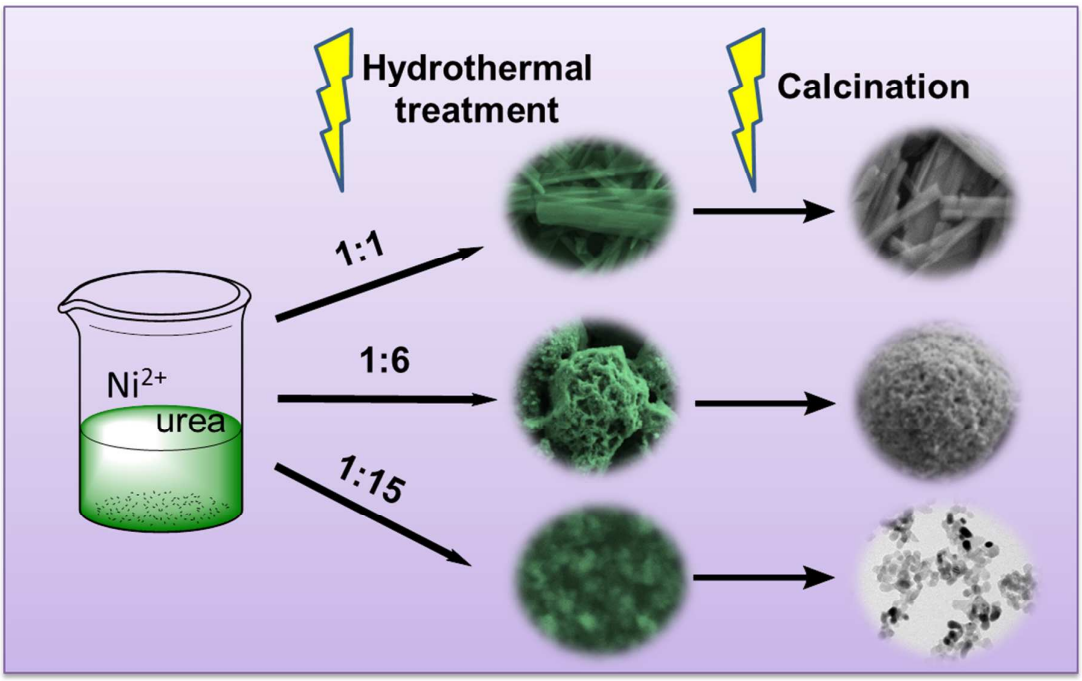

Scheme 1 Illustration for the synthesis of NiO nanostructures with different morphologies from the obtained Ni-based nanoprecursors prepared via a urea-controlled hydrothermal method.

3. Results and discussion

The phase purity and crystal structure of the products obtained with different mole ratios of $NiSO_4{\cdot}(NH_4)_2SO_4{\cdot}6H_2O$/urea were examined by XRD patterns and SEM images. Fig. 1a shows the XRD pattern of the sample (P1) prepared when the mole ratio of $NiSO_4{\cdot}(NH_4)_2SO_4{\cdot}6H_2O$/urea is 1:1. All of the diffraction peaks could be perfectly indexed to pure $Ni(SO_4)_{0.3}(OH)_{1.4}$ (JCPDS Card No. 41–1424). No other diffraction peaks were detected, demonstrating the high purity of $Ni(SO_4)_{0.3}(OH)_{1.4}$. The morphologies of the as-prepared $Ni(SO_4)_{0.3}(OH)_{1.4}$ sample (P1) were studied by SEM. As shown in Fig. 1b and c, a large quantity of belt-like structures with a typical length of several micrometers and a width of about 100 nm was obtained. When decreasing the mole ratio of $NiSO_4{\cdot}(NH_4)_2SO_4{\cdot}6H_2O$/urea to 1:6, as shown in Fig. 1d, the XRD pattern of sample P2 shows that the as-fabricated products belong to the crystal phase of $Ni(HCO_3)_2$ (JCPDS No. 15-782). The broaden diffraction peaks indicte the sample is composed of large scale of fine $Ni(HCO_3)_2$ nanocrysrtals. Fig. 1e and f show that the prepared $Ni(HCO_3)_2$ consists of many microspheres, which is assembled with small nanoparticles. While the mole ratio of $NiSO_4{\cdot}(NH_4)_2SO_4{\cdot}6H_2O$/urea is adjusted to 1:15, as dipicted in the XRD pattern (Fig. 1g) and SEM images (Fig. 1h and i), it can be clearly seen that a large amount of $Ni(HCO_3)_2$ nanoparticles was fabricated.

Based on the above results, $Ni(SO_4)_{0.3}(OH)_{1.4}$ and $Ni(HCO_3)_2$ nanostructures precursors can be selectively prepared in the mixed $NiSO_4{\cdot}(NH_4)_2SO_4{\cdot}6H_2O$-urea-$H_2O$ system via tuning the amounts of urea. It is well known that the decomposition of urea results in the release of CO_3^{2-} and NH_4^+, which could generate HCO_3^- and OH^- through the hydrolysis process. In the present reaction system, it was proposed at lower urea amounts of 2 mmol (the mole ratio of $NiSO_4{\cdot}(NH_4)_2SO_4{\cdot}6H_2O$/urea is 1:1), the generation of OH^- is predominant, leading to the formation of $Ni(SO_4)_{0.3}(OH)_{1.4}$. Yang et al.[21] and Wen et al.[20] also pointed out that the gradual release of OH^- from hydrolysis of the acetate plays a key role in the formation of one dimensional (needle-like and belt-like) $Ni(SO_4)_{0.3}(OH)_{1.4}$ nanostructures. When the amount of urea is increased to 12 mmol (the mole ratio of $NiSO_4{\cdot}(NH_4)_2SO_4{\cdot}6H_2O$/urea to 1:6), HCO_3^- would be produced and then result in the precipitate of $Ni(HCO_3)_2$. Interestingly, the product is not well-crystallized according to the XRD pattern, which might be due to not enough CO_2 will react with CO_3^{2-} forming HCO_3^-, resulting in poor-crystallized $Ni(HCO_3)_2$ phase.[22] While the mole ratio of $NiSO_4{\cdot}(NH_4)_2SO_4{\cdot}6H_2O$/urea is adjusted to 1:15, the generation of large amounts of HCO_3^- predominantly occurs during the ureolysis, resulting in the formation of well-crystallized $Ni(HCO_3)_2$ phase.

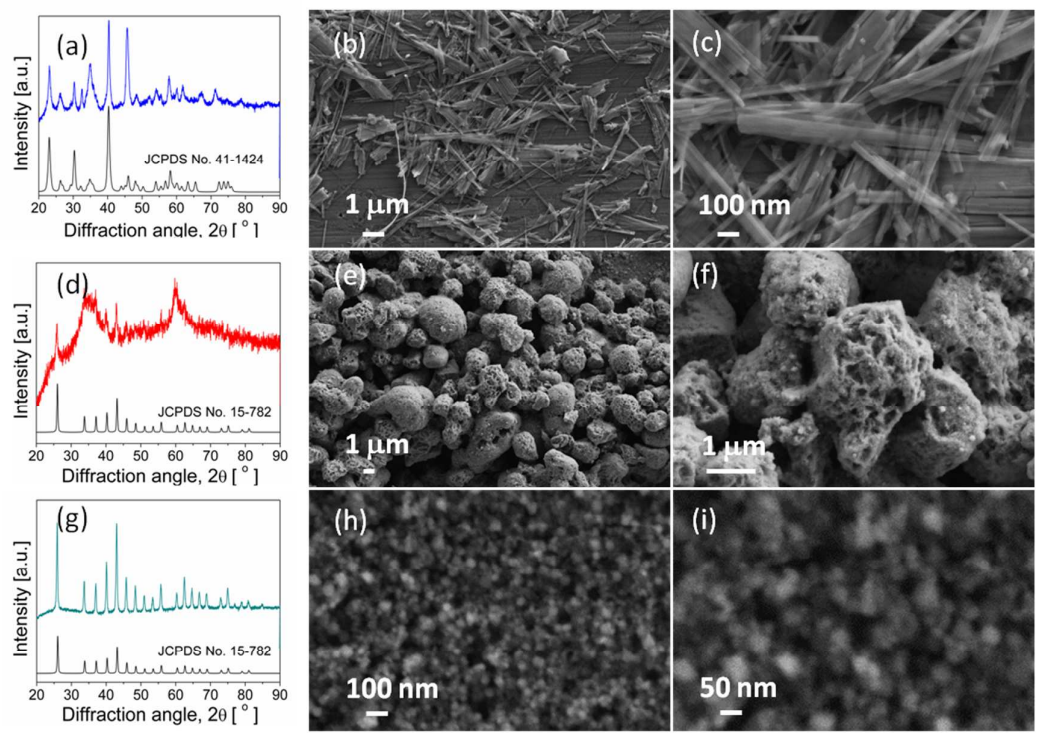

Fig. 1 XRD patterns (a, d, and g) and SEM images (b, c, e, f, h, and i) of the as-synthesized products (P1, P2, and P3) with different mole ratios of $NiSO_4 \cdot (NH_4)_2SO_4 \cdot 6H_2O$/urea: P1 (a-c), P2 (d-f), and P3 (g-i).

In brief, the morphology tailoring of NiO nanostructures involves the calcining of Ni-based nanostructure precursors at 450°C for 2 h. Fig. 2 shows the XRD patterns of the as-obtained samples synthesized by a calcination treatment of $Ni(SO_4)_{0.3}(OH)_{1.4}$ and $Ni(HCO_3)_2$ nanostructures precursors. Their diffraction peaks correspond to the (222), (311), (220), (200), and (111) planes, respectively. All the diffraction peaks could be perfectly indexed to the face-centered cubic phase (space group *Fm3m*) NiO (JCPDS Card No. 73-1523). No other diffraction peak was detected, indicating that pure NiO crystals have been successfully fabricated.

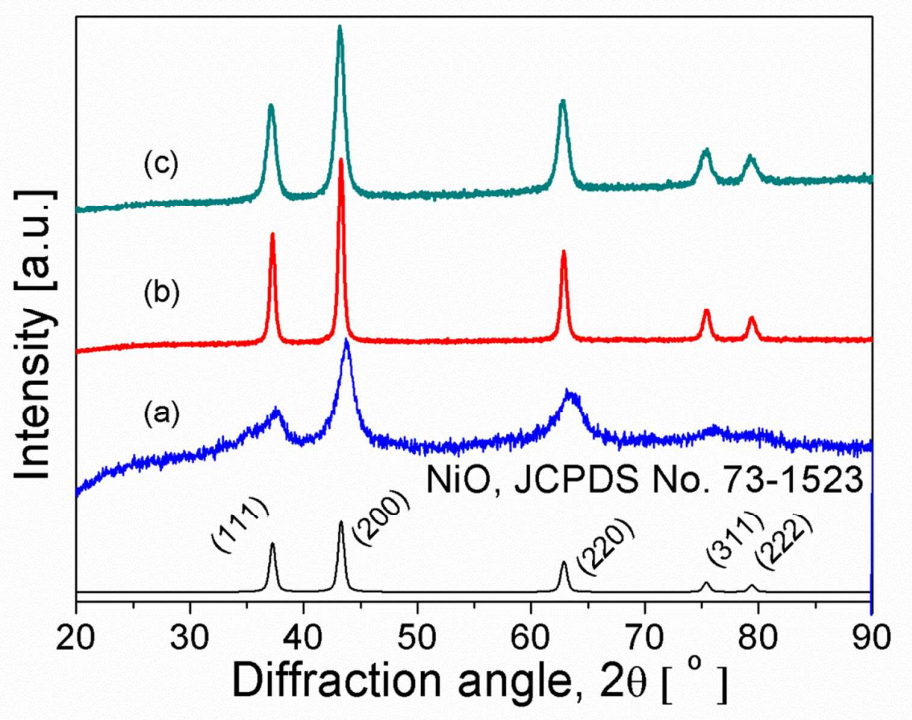

Fig. 2 XRD patterns of the obtained samples synthesized by calcining of different Ni-based precursors: (a) P1, $Ni(SO_4)_{0.3}(OH)_{1.4}$ nanobelts, (b) $Ni(HCO_3)_2$ nanospheres, (c) $Ni(HCO_3)_2$ nanoparticles.

Fig. 3 shows the TGA curves of $Ni(SO_4)_{0.3}(OH)_{1.4}$ nanobelts, $Ni(HCO_3)_2$ nanospheres, and $Ni(HCO_3)_2$ nanoparticles. It was observed that NiO was transformed with calcinations treatment of $Ni(HCO_3)_2$ phase at 450°C for 2 h. Zhang et al.[23] found NiO was obtained and still keep the same morphology with $Ni(SO_4)_{0.3}(OH)_{1.4}$ after heat treatment of $Ni(SO_4)_{0.3}(OH)_{1.4}$ at 500 °C. As the heat treatment temperature increased to 750 °C, the belt-like $Ni(SO_4)_{0.3}(OH)_{1.4}$ was completely destroyed and transformed into agglomerated NiO nanoparticles with random orientation but better crystallinity. However, in the present system, the $Ni(SO_4)_{0.3}(OH)_{1.4}$ nanobelts still have weight loss when the calcining temperature is higher than 450°C, which is good agreement with Wen et al. reported.[20] From the XRD result, it was observed that the peaks of NiO products prepared by calcining of $Ni(SO_4)_{0.3}(OH)_{1.4}$ have slight shift, which might be due to the lower calcining temperature for $Ni(SO_4)_{0.3}(OH)_{1.4}$.[20] Furhter study on tunable synthesis of $Ni(SO_4)_{0.3}(OH)_{1.4}$ nanostructures and their transformation to NiO nanomaterials by calcining process is still in progress.

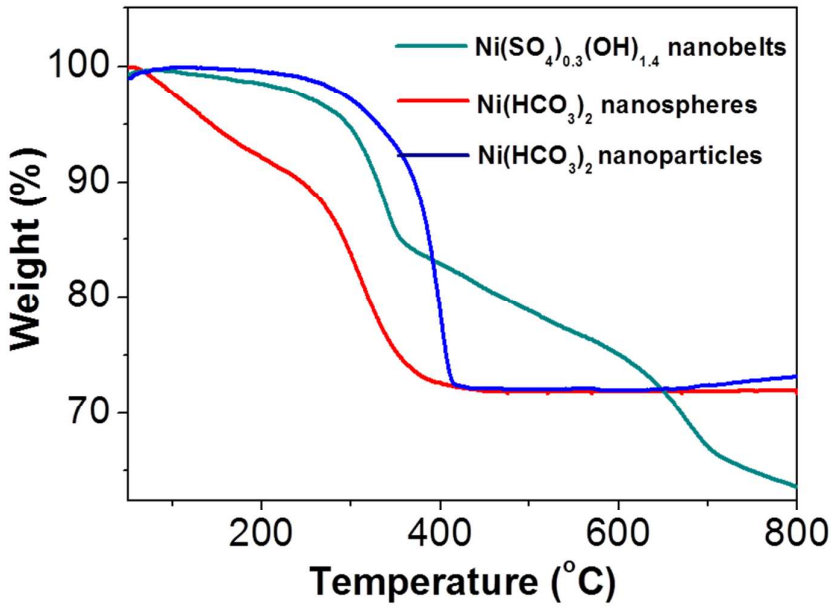

Fig. 3 TGA curves of $Ni(SO_4)_{0.3}(OH)_{1.4}$ nanobelts, $Ni(HCO_3)_2$ nanospheres, and $Ni(HCO_3)_2$ nanoparticles.

Electron microscopy was used to further characterize the changes in morphology and structure associated with calcinations of the as-prepared Ni-based nanostructures precursors. It is clearly seen that the as-synthesized NiO powders retained the dimensional structure and morphology of the Ni-based precursors based on the SEM images and TEM image (Fig. 4). As shown in Fig. 4a and b, plenty of NiO nanobelts were obtained when using belt-like $Ni(SO_4)_{0.3}(OH)_{1.4}$ products as the precursor. While employing spherical $Ni(HCO_3)_2$ nanostructures as the precursor, as displayed in Fig. 4c and d, NiO nanospheres composed of small nanoparticles were fabricated. Fig. 4e and f show that a large number of NiO nanoparticles with diameter of 30 nm were prepared with the calcination treatment of $Ni(HCO_3)_2$ nanoparticles at 450°C for 2 h. On the basis of the above observation, NiO nanostructures with different morphologies have been successfully synthesized by using different Ni-based nanostructures precursors prepared via a urea involved hydrothermal method, as shown in Scheme 1. In this synthesis, Ni-based nanoprecursors were employed as hard templates, directing the formation of different shaped NiO nanostructures by calcining treatment.

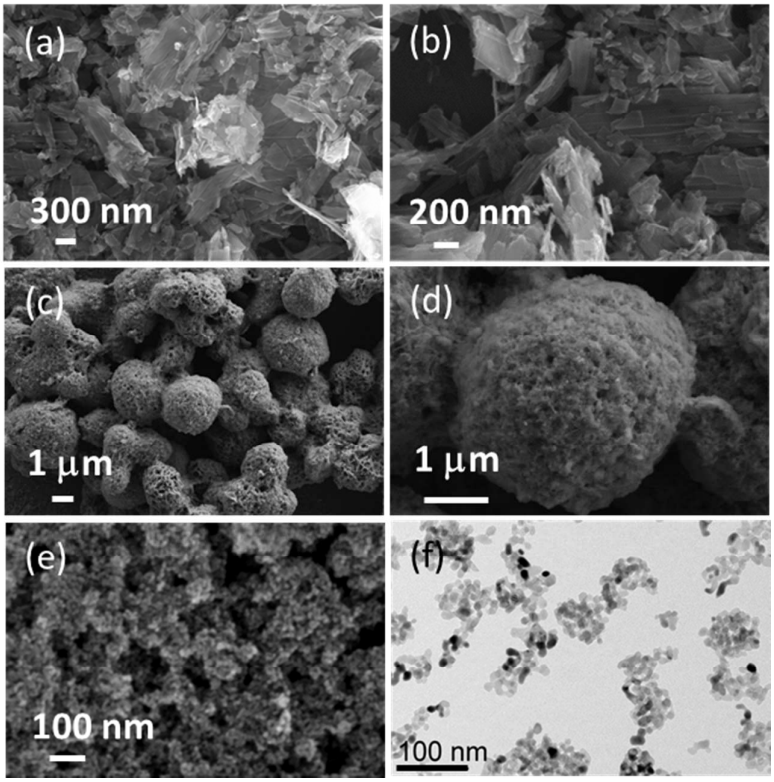

Fig. 4 SEM (a-e) images and TEM image (f) of the obtained samples synthesized by calcining of different Ni-base precursors: (a and b) P1, $Ni(SO_4)_{0.3}(OH)_{1.4}$ nanobelts, (c and d) $Ni(HCO_3)_2$ nanospheres, (e and f) $Ni(HCO_3)_2$ nanoparticles.

Fig. 5 shows the nitrogen adsorption–desorption isotherms of different NiO nanostructures to determine the BET specific surface areas by nitrogen adsorption–desorption measurements. The BET surface areas of the as-prepared NiO nanobelts, nanospheres, and nanoparticles were 44.2, 18.1, and 58.5 m^2 g^{-1}, respectively. The as-synthesized NiO materials demonstrated different BET surface areas, which is attribute to the differences in their structures, as shown by the SEM and TEM images. The pore size distribution of three kinds of NiO was determined by using the Barret–Joyner–Halenda (BJH) method. It can be observed that NiO nanoparticles contained small mesopores, which may be ascribed to the aggregation of nanoparticles during the calcinations process. The BET specific surface areas of the NiO nanoparticles demonstrate that the nanoparticulate structure of NiO has a relatively high surface-to-volume ratio, which is helpful for the electrochemical performance.[24, 25]

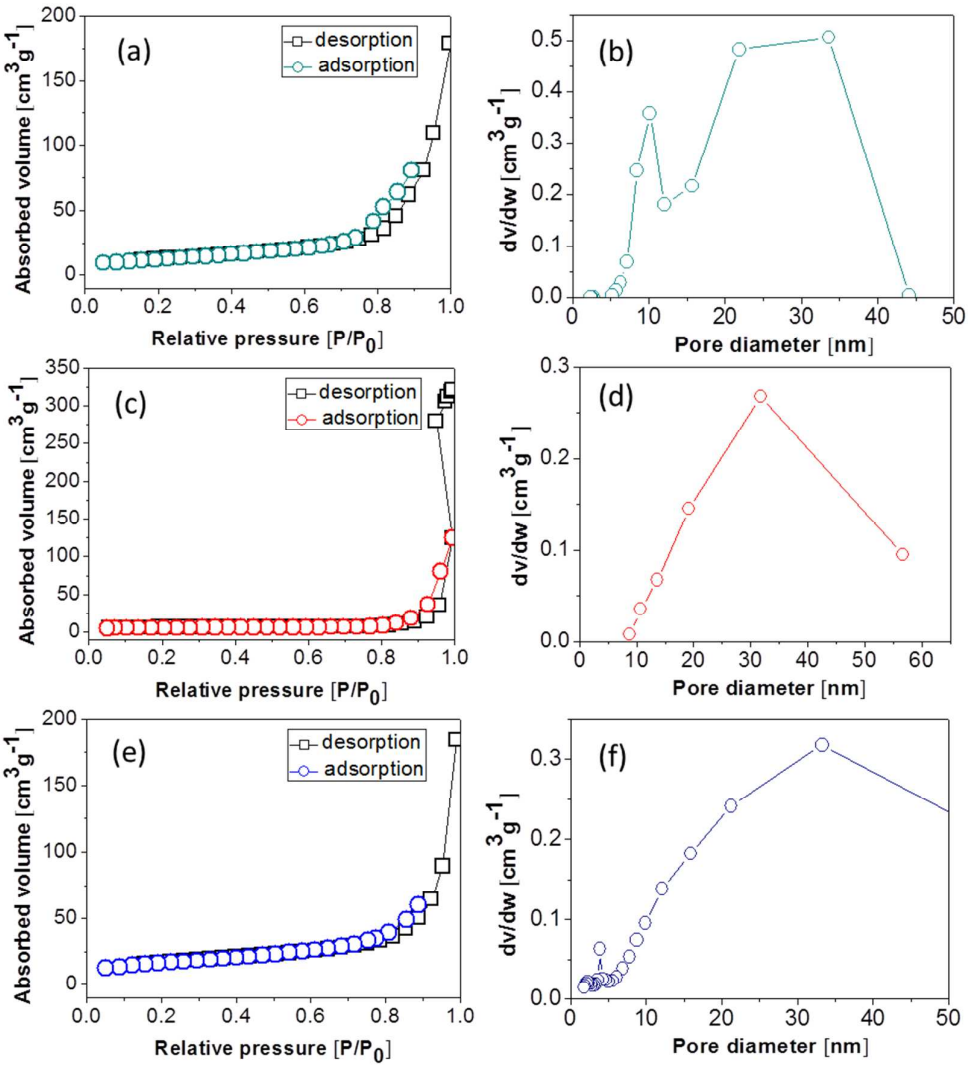

Fig. 5 Nitrogen adsorption–desorption isotherms (a, c and e) and pore size distribution (b, d and f) of NiO samples: (a and b) nanobelts, (c and d) nanospheres, (e and f) nanoparticles.

The capacity performances of the as-synthesized NiO nanobelts, nanoparticles, and nanospheres were investigated in 6 M KOH. Fig. 6a shows the cyclic voltammetry (CV) curves scanned at 10 mV s^{-1} of three different kinds of NiO electrodes. Faradic pseudo-activity induced capacitance was reflected by a pair of strong symmetry redox peaks in each CV curve. It was observed the anodic peaks were in the range of 0.25~0.4 V, which could be attributed to the reduction of NiO into NiOOH, while the catholic peaks at 0.0~0.1 V is related with the conversion of NiOOH back to NiO. The charge storage of NiO arises from the following redox equation:[5, 9, 26]

$$NiO + OH^- \underset{\text{discharge}}{\overset{\text{charge}}{\rightleftharpoons}} NiOOH + e^-$$

The galvanic charge-discharge curves at the current density of 5 A g^{-1} within the voltage range of -0.2~0.5 V is shown in Fig. 6b. The flat stage in the charge/discharge curve clearly demonstrates the pseudo-capacitance was induced by faradaic charges. The specific capacitances of NiO nanospheres, nanobelts, and nanoparticles calculated from CV curves are 45.2, 556.2, and 609.5 F g^{-1}, respectively. The duration of galvanic charge/discharge cycle is in good agreement with CV measurements.

In our experiment, judging from the XRD pattern in Fig. 2, NiO nanobelts derived from the calcination of $Ni(SO_4)_{0.3}(OH)_{1.4}$ have poor crystallization compared with another two samples derived from the calcination of $Ni(HCO_3)_2$. Consequently, reflected in electrochemical figures, the as-made samples from calcination of $Ni(HCO_3)_2$ shows better symmetric features in cyclic voltammetry curve. The catholic shift is due to the different crystallinity in calcinated samples, where ions are charged and discharged continuously and the electrolyte diffuses, inducing ohmic resistance and polarization. The crystallinity alteration resulting in different redox peak positions were also found in previously published papers.[5, 27]

The capacitive performances of nickel oxide are affected by main factors such as particle size, surface area and morphologies.[24, 25] As for the pseudo-capacitive materials, the shrinked particle size and enlarged surface area are substantially helpful in augmenting the amount of electrons in valence-reversible faradaic reaction. Among the three different kinds of nanostructures, NiO nanoparticles show the largest BET surface area, which could lead to improved electrolyte permeability and facilitates the enhancement of electron pathways, thus potentially improving the pseudocapacitance.[27] For current corrective acetylene black, it was difficult to go into the inner space of the big NiO spheres, resulting in a low electron-transfer efficiency induced by uniform dispersion of acetylene black in nanospheres, which greatly compromised the electrochemical performance of nanospheres. Reflected in the cyclic voltammetry and galvanic charge-discharge, the curves of nanobelt and nanoparticle covers bigger area than that of nanospheres, which is in good agreement with the sequence of surface area analysis.

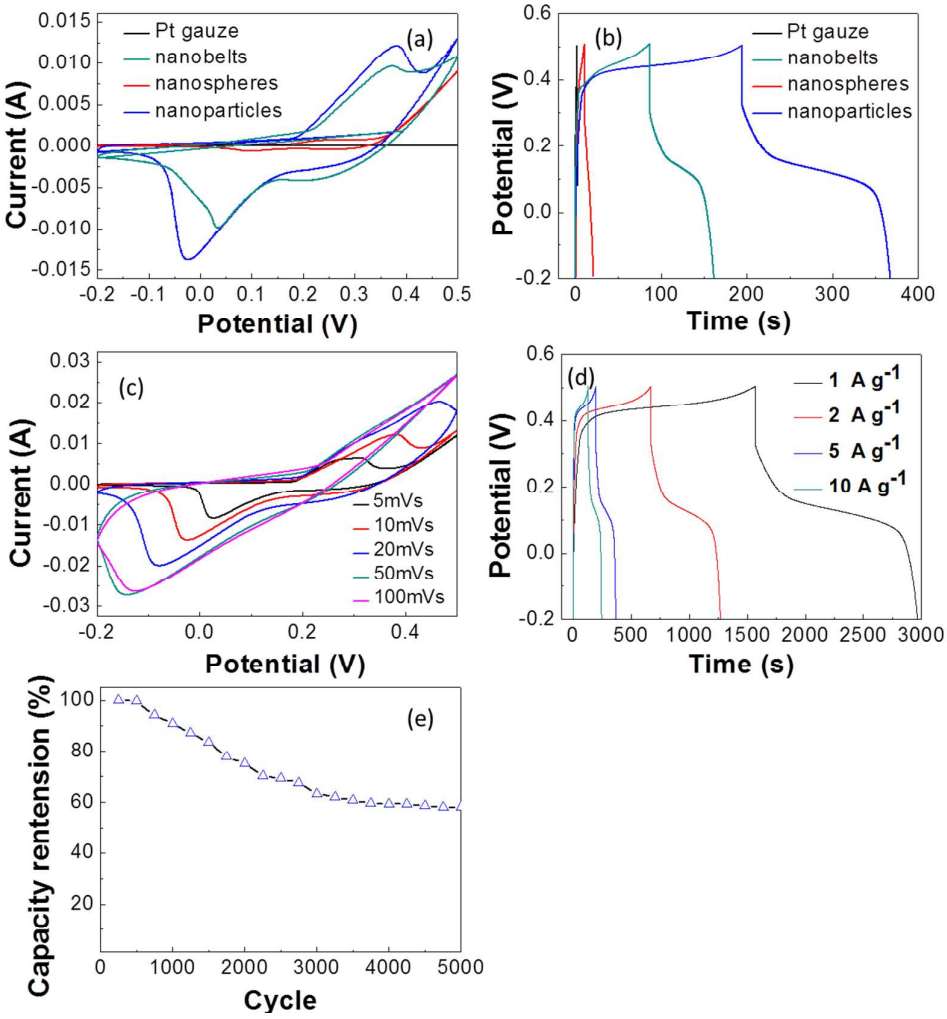

Fig. 6 The cyclic voltammetry curves (a) and galvanic charge/discharge curves (b) of NiO nanobelts, nanospheres, and nanoparticles, (c) cyclic voltammetry of NiO nanoparticles at different scan rates, (d) cyclic voltammetry of NiO nanoparticles at different current density, (e) the capacitance stability of NiO nanoparticles at the constant current density of 5 A g^{-1}.

On the basis of these morphological studies, cyclic voltammogram tests on the NiO nanoparticles as active materials for a supercapacitor were performed at different scan rates to observe the CV curve change, as shown in Fig. 6c. A gradual increase in current density was observed in the redox CV curves with an increase in the scan rate, indicating that the electrochemical process was surface confined. In addition, within the increase of scan rate, the anodic peak potential and catholic peak potential shift positively and negatively, respectively, while the capacitance decreases as elevated scan rates higher than 50mv s^{-1}. As shown in Fig. 6d, the specific capacitance of NiO nanoparticles at different current density is provided, in which the current density is 0.5A g^{-1}, 1 A g^{-1}, 5 Ag^{-1} and 10 A g^{-1}, respectively.

From the experimental results, it can be concluded that the increase of current density dwarfs the performance of specific capacitance of samples (calculated as 770.5F g^{-1}, 680.4 F g^{-1}, 609.5 F g^{-1} and 524.4 F g^{-1}, respectively).

The cyclic stability of NiO nanoparticles after 5000 repeated cycles is shown in Fig. 6e. It was found that there was no capacity shrinks in the first 500 cycles, while there was a drastic capacity decrease from 500 to 3000 cycles. It was observed that the capacity was stabilized by 3750 cycles and only ~62% of the original specific capacitance was retained, which might due to the detachment of NiO nanoparticles from the current collectors. It was previously reported that the capacitance of NiO nanomaterials is generally between 69.8 and 285 F g^{-1}.[28-31] The above results suggest that the as-synthesized NiO nanoparticles have relatively high supercapacitances and excellent capacitance retention.

4. Conclusion

In summary, by tuning the amounts of urea, $Ni(SO_4)_{0.3}(OH)_{1.4}$ and $Ni(HCO_3)_2$ nanostructures precursors were selectively synthesized in water via a facile hydrothermal method. After thermal treatment, different nanostructured $Ni(SO_4)_{0.3}(OH)_{1.4}$ and $Ni(HCO_3)_2$ can be converted into NiO nanobelts, nanospheres, and nanoparticles, which show different BET surface areas. The electrochemical measurements of three kinds of different NiO nanostructures-based supercapacitors revealed that NiO nanoparticles exhibit pseudo-capacitive properties with high capacitance and good capacitance retention, which probably benefit from the structural features of being nanoparticulate and large surface areas.

Notes

The authors declare no competing financial interest.

References

1. H. Jiang, J. Ma and C. Li, *Adv. Mater.*, 2012, 24, 4197-4202.
2. X. Lu, D. Zheng, T. Zhai, Z. Liu, Y. Huang, S. Xie and Y. Tong, *Energy Environ. Sci.*, 2011, 4, 2915-2921.
3. L. Feng, Y. Zhu, H. Ding and C. Ni, *J. Power Sources*, 2014, 267, 430-444.
4. B. Wang, J. S. Chen, Z. Wang, S. Madhavi and X. W. Lou, *Adv. Energy Mater.*, 2012, 2, 1188-1192.
5. K. K. Purushothaman, I. Manohara Babu, B. Sethuraman and G. Muralidharan, *ACS Appl. Mater. Interfaces*, 2013, 5, 10767-10773.
6. G. Zhang, L. Yu, H. E. Hoster and X. W. Lou, *Nanoscale*, 2013, 5, 877-881.

7. W. Yu, X. Jiang, S. Ding and B. Q. Li, *J. Power Sources*, 2014, 256, 440-448.
8. Z. Yang, F. Xu, W. Zhang, Z. Mei, B. Pei and X. Zhu, *J. Power Sources*, 2014, 246, 24-31.
9. S. K. Meher, P. Justin and G. Ranga Rao, *Nanoscale*, 2011, 3, 683-692.
10. Y. Wang, Q. Zhu and H. Zhang, *Chem. Commun.*, 2005, 5231-5233.
11. X. Wan, M. Yuan, S.-l. Tie and S. Lan, *Appl. Surf. Sci.*, 2013, 277, 40-46.
12. Y. Cui, C. Wang, S. Wu, G. Liu, F. Zhang and T. Wang, *CrystEngComm*, 2011, 13, 4930-4934.
13. S. Vijayakumar, S. Nagamuthu and G. Muralidharan, *ACS Appl. Mater. Interfaces*, 2013, 5, 2188-2196.
14. X. Tian, C. Cheng, L. Qian, B. Zheng, H. Yuan, S. Xie, D. Xiao and M. M. F. Choi, *J. Mater. Chem.*, 2012, 22, 8029-8035.
15. T. Alammar, O. Shekhah, J. Wohlgemuth and A.-V. Mudring, *J. Mater. Chem.*, 2012, 22, 18252-18260.
16. J. H. Pan, Q. Huang, Z. Y. Koh, D. Neo, X. Z. Wang and Q. Wang, *ACS Appl. Mater. Interfaces*, 2013, 5, 6292-6299.
17. J. Li, F. Luo, Q. Zhao, Z. Li, H. Yuan and D. Xiao, *J. Mater. Chem. A*, 2014, 2, 4690-4697.
18. R. Wang, Q. Li, D. Xie, H. Xiao and H. Lu, *Appl. Surf. Sci.*, 2013, 279, 129-136.
19. S. Ding, T. Zhu, J. S. Chen, Z. Wang, C. Yuan and X. W. Lou, *J. Mater. Chem.*, 2011, 21, 6602-6606.
20. W. Wen, J.-M. Wu, L.-L. Lai, G.-P. Ling and M.-H. Cao, *CrystEngComm*, 2012, 14, 6565-6572.
21. D. Yang, P. Liu, Y. Gao, H. Wu, Y. Cao, Q. Xiao and H. Li, *J. Mater. Chem.*, 2012, 22, 7224-7231.
22. Y. Yan, G. Cheng, P. Wang, D. He and R. Chen, *RSC Adv.*, 2014, 4, 49303-49307.
23. K. Zhang, J. Wang, X. Lu, L. Li, Y. Tang and Z. Jia, *J Phys Chem C*, 2009, 113, 142-147.
24. S. Chen, W. Xing, J. Duan, X. Hu and S. Z. Qiao, *J. Mater. Chem. A*, 2013, 1, 2941-2954.
25. R. B. Rakhi, N. A. Alhebshi, D. H. Anjum and H. N. Alshareef, *J. Mater. Chem. A*, 2014, 2, 16190-16198.
26. S. Xiong, C. Yuan, X. Zhang and Y. Qian, *CrystEngComm*, 2011, 13, 626-632.
27. S.-I. Kim, J.-S. Lee, H.-J. Ahn, H.-K. Song and J.-H. Jang, *ACS Appl. Mater. Interfaces*, 2013, 5, 1596-1603.
28. Y.-g. Wang and Y.-y. Xia, *Electrochim. Acta*, 2006, 51, 3223-3227.
29. X. Zhang, W. Shi, J. Zhu, W. Zhao, J. Ma, S. Mhaisalkar, T. Maria, Y. Yang, H. Zhang, H. Hng and Q. Yan, *Nano Res.*, 2010, 3, 643-652.
30. A. I. Inamdar, Y. Kim, S. M. Pawar, J. H. Kim, H. Im and H. Kim, *J. Power Sources*, 2011, 196, 2393-2397.
31. Y.-z. Zheng, H.-y. Ding and M.-l. Zhang, *Mater. Res. Bull.*, 2009, 44, 403-407.